

Chapter 4:
Biochemical and Biophysical
Characterization of the LHC Protein
Aggregates

Abstract

Protein aggregation is detrimental to cells. To overcome this problem, cells have evolved specialized chaperone systems to reverse existing protein aggregates; these “disaggregases” are often ATP-dependent macromolecular machines. Recently, we found that the 43-kDa subunit of chloroplast Signal Recognition Particle (cpSRP43) can efficiently reverse the aggregation of its substrate proteins, the light-harvesting chlorophyll a/b-binding (LHC) proteins, in the absence of external energy input. To understand the molecular mechanism of this novel disaggregase activity, it is imperative to first know the nature of the protein aggregates handled by cpSRP43. Using biophysical and biochemical methods, we found that LHC proteins form disc-shaped aggregates ~ 12 nm in diameter and 1–2 nm in height. They contain exposed hydrophobic grooves that could be probed by a variety of small fluorescent dyes. LHC protein aggregates are kinetically stable and resistant to detergents, but can be resolubilized by strong chemical denaturants. These observations provide important clues to understanding the capability and specificity of cpSRP43’s disaggregase activity.

Introduction

The proper folding of proteins into their three-dimensional structures is essential for their function. *In vivo*, many factors pose challenges to protein folding, including environmental stress and molecular crowding (1). Within this setting, improper intra- or intermolecular interactions can occur and lead to the aggregation of proteins. Protein aggregation is detrimental to cells as it deprives the cells of functional proteins. Moreover, some aggregates, most notoriously those that form amyloid fibrils, are toxic to cells and cause numerous protein-folding diseases (2).

Despite early suggestions that protein aggregates are amorphous (3), emerging evidence has argued for some degrees of order and specificity in aggregate formation (4). For instance, folding intermediates of bovine growth hormone, phosphoglycerate kinase, P22 tailspike, and coat proteins have been shown to participate in specific intermolecular interactions in their aggregation pathways (5, 6). The extreme case of ordered protein aggregates is the amyloid fibrils, which form extensive cross- β strand structures (7). Many techniques have been developed to map out the structures of protein aggregates, especially the various intermediates during amyloid fibril formation. For example, transmission electron microscopy (TEM) and high-resolution atomic force microscopy (AFM) reveal global size, shape, and morphology of the aggregates (8, 9). Scanning transmission electron microscopy (STEM) can provide an estimate of the mass and/or density of the aggregates (10). Fluorescent small molecule dyes probe the presence of β -sheet structures or exposed hydrophobic patches in the aggregates (11, 12). Because of their unconventional order, the amyloid fibrils can be crystallized, and their X-ray crystal structures provide unprecedented resolution in visualization of protein aggregates (7, 13).

These powerful techniques reveal that protein aggregates can form highly-ordered structures that are thermodynamically and kinetically stable and contain specific intra- or intermolecular interactions that are not trivial to break.

Nevertheless, cells have evolved ways to handle protein aggregates. A specialized class of molecular chaperones, the disaggregases, can perform an energetically uphill process of reversing protein aggregation. The most well-characterized disaggregases belong to the Clp/Hsp100 family of AAA+ ATPases (ATPases associated with various cellular activities), such as ClpB in prokaryotes and Hsp104 in yeasts (*14*). Both are large hexameric rings that are powered by mechanical forces from ATP hydrolysis, and both require additional co-chaperones to efficiently dismantle protein aggregates (*15, 16*). These disaggregases are capable of reversing the aggregation of many model proteins. The complexity of these disaggregase systems and the promiscuity in their substrate selection have made it difficult to pinpoint their molecular mechanisms of action.

Recently, we found an efficient disaggregase activity in the 43-kDa subunit of the chloroplast Signal Recognition Particle (cpSRP43) (*17*). Unlike the Clp/Hsp100 family of disaggregases, cpSRP43 is a highly specific chaperone/disaggregase for its substrates, the light-harvesting chlorophyll a/b-binding (LHC) proteins (*18*). LHC proteins are synthesized in the cytosol and are likely unfolded when they enter the chloroplast, where they are recognized and delivered to the thylakoid membrane by the cpSRP (*18*). LHC proteins are highly hydrophobic proteins containing three transmembrane (TM) helices (*19*). A well-conserved 18-amino acid loop between the second and the third TM helices, termed L18, provides a specific recognition element for high affinity binding by

cpSRP43 (17, 20, 21). In previous work we showed that the specific interaction of cpSRP43 with the L18 motif is crucial for the disaggregation activity of cpSRP43. This and other observations led us to propose that, in the absence of external energy input, cpSRP43 uses specific binding energy with its substrate protein to drive its disaggregase activity (17).

To understand the molecular mechanism that underlies cpSRP43's novel disaggregase activity, we need to understand the nature of the LHC protein aggregate that cpSRP43 recognizes and subsequently remodels. What does it look like? What is presented outside of the aggregate to enable its recognition by cpSRP43? How strong are the internal packing interactions of the aggregate, which need to be overcome by the disaggregase? This chapter aims to answer some of these questions via several biochemical and biophysical methods. We found that the LHCP aggregates are disc-like particles that are ~ 12 nm wide and 1–2 nm thick. They have exposed hydrophobic patches that could bind to environmentally sensitive fluorescent dyes. Additionally, we investigated the stability of the aggregates using various detergents and chemical denaturants.

Results

LHCP forms stable, micellar aggregates.

Previously, we developed an assay for the formation of large LHCP aggregates based on light scattering (17). At LHCP concentrations above ~ 100 nM, there was a linear relationship between the light scattering intensity and the concentration of LHCP (Figure 4.1A, black), suggesting that aggregation was complete under these conditions. However, the linearity broke down at LHCP concentrations below 100 nM (Figure 4.1A and inset, black). This was not because of limitations in instrument sensitivity; when pre-formed LHCP aggregates were serially diluted, linearity in light scattering intensity was observed throughout the entire concentration range and extrapolated through the zero point (Figure 4.1A inset, red). These observations showed that: (i) the LHCP aggregate is kinetically stable and virtually irreversible once it has formed; and (ii) formation of the LHCP aggregate involves a lag phase below a critical protein concentration, which is reminiscent of the critical micellar concentration (CMC) during the formation of micelles. Based on this information, we estimated the CMC values for aggregate formation by LHCP and a number of LHCP variants as the X-intercepts from linear fits to data (Figure 4.1A and B; (22)). These analyses yielded CMC values of 100–200 nM for the different LHCP aggregates (Figure 4.1B).

LHCPs form disc-shaped aggregates with diameters of ~ 12 nm.

To investigate the global structure of the aggregate formed by LHCP, we employed TEM and AFM. The negatively stained TEM images revealed LHCP aggregates to be circular particles with diameters of 12 ± 2 nm (Figure 4.2). Consistent

with the EM images, AFM analysis also showed LHCP aggregates to be disc-shaped particles (Figure 4.3A). Analysis of the area of these particles resulted in a distribution that could be fit with a Gaussian function, giving a peak at 214 nm² (Figure 4.3B). Assuming that LHCP aggregates were circular in shape, the diameter estimated from the mean area was 16±5 nm, in good agreement with the EM measurements. The heights of the LHCP aggregates measured by AFM were in the range of 1–2 nm (Figures 4.3C and D).

LHCP aggregates contain exposed hydrophobic grooves.

Many protein aggregates contain exposed hydrophobic microdomains that could be probed by small-molecule fluorescent dyes such as 1-anilino-8-naphthalene sulfonate (ANS) and bis-ANS, as the fluorescence intensity of these dyes increases upon exposure to a non-polar environment (12). We asked whether the LHCP aggregates share this feature with other aggregates. Indeed, the fluorescence of both ANS (not shown) and bis-ANS (Figure 4.4A) increased significantly upon the addition of 1µM LHCP aggregate, accompanied by a blue shift of the fluorescence emission spectra (Figure 4.4A). These results strongly suggested that the LHCP aggregate contains exposed hydrophobic microdomains that allow the binding of these dyes, consistent with the highly hydrophobic nature of this protein.

We also used Thioflavin T (ThT) to probe the structural organization of the LHCP aggregate. ThT is an environmentally sensitive fluorescent dye that is often used as a diagnostic for the formation of amyloid fibrils generated by amyloid-β (Aβ), α-synuclein, and other amyloidogenic proteins (11). Similar to bis-ANS, the fluorescence of ThT also

exhibited a significant increase in intensity and a blue shift in its spectrum in the presence of the LHCP aggregate (Figure 4.4B, blue lines). The extent of these fluorescence changes are comparable to that induced by mature amyloid fibrils generated from the amyloid- β peptide (Figure 4.4B, red vs. blue, and Figure 4.4C). As both the TEM and AFM analyses did not indicate amyloid formation in the LHCP aggregate (see above), these results support suggestions from recent work that ThT is not highly specific for amyloid fibrils. Instead, this dye possibly binds to hydrophobic grooves that are often present in amyloid fibrils but can also be generated by other types of aggregates (23).

LHCP aggregates are detergent-resistant but can be solubilized by strong chemical denaturants.

In order to reverse aggregation, cpSRP43 must overcome the packing interactions that stabilize the LHCP aggregate. To probe the stability of this aggregate, we tested whether it could be solubilized by various detergents, including n-Dodecyl-N,N,-Dimethylamine-N-Oxide (LDAO), n-Dodecyl- β -D-Maltopyranoside (DDM), Triton X-100 (TX-100), n-Nonyl- β -D-Glucopyranoside (BNG), and n-Octyl- β -D-Glucopyranoside (β -OG). The results of the sedimentation assay (see Methods) showed that none of these detergents were able to solubilize the LHCP aggregate at or above the concentrations used for membrane protein solubilization (Figure 4.5A). Sodium dodecyl sulfate (SDS) could completely solubilize the LHCP aggregate, as LHCP is present in the soluble fraction after incubation with SDS for 30 minutes (Figure 4.5B, left panel).

We also tested SDS solubility of the LHCP aggregate using an established protocol for amyloid fibrils (24). Unlike the sedimentation assay in which centrifugation

is used to separate pellet and soluble fractions after incubation with the detergents, this assay judges solubility of the aggregate by the mobility of the proteins into the separating gel after incubation with the SDS-containing buffer at room temperature ((24); see Methods). The solubilized amyloid fibrils can migrate into the separating gel without boiling, whereas the aggregates cannot enter into the separating gel unless boiled (24). Based on this standard, LHCP aggregate showed partial resistance to 2% SDS as only 24% of the aggregates could migrate into the gel without boiling (Figure 4.5B).

Inspired by the insights gained from quantitative analyses of protein unfolding by chemical denaturants, we also probed the stability of the LHCP aggregate by analyzing its solubility in chemical denaturants. Using the sedimentation assay, we showed that both guanidinium hydrochloride (GdmHCl) and urea could effectively solubilize the LHCP aggregates in a concentration-dependent manner (Figure 4.6A). Quantification of the amount of solubilized LHCP as a function of urea concentration gave an aggregate solubilization curve analogous to the protein denaturation curves (Figure 4.6B). Based on a two-state model, quantitative analyses of these data yielded information about the energetics of transfer of LHCP from urea to water (ΔG°) and the urea concentration required to achieve 50% solubilization (U_{50} ; see Methods). These parameters provide quantitative empirical measures of the energetics of the internal packing interactions that stabilize the LHCP aggregate. In summary, the results in this section demonstrate that LHCP forms stable aggregates that are resistant to various detergents, but could be dissolved by strong chemical denaturants such as SDS, GdmHCl, and urea.

Discussion

To understand the molecular mechanism of cpSRP43's disaggregase activity, it is essential to understand the nature of its substrate, the LHCP aggregate. Many techniques have been employed to characterize the LHCP aggregates. We found that LHCP forms disc-shaped aggregates ~ 12 nm in diameter and 1–2 nm in thickness. The aggregates contain exposed hydrophobic surfaces as probed by several environmentally sensitive small molecule dyes. Further, analyses of aggregate formation and solubilization suggest that LHCP forms micelle-like aggregates that are thermodynamically and kinetically stable.

It is interesting to note that the morphology of the LHCP aggregates bears some resemblance to the soluble oligomeric intermediates that precede the amyloid fibril formation, which are often disc-shaped, 9–25 nm in diameter and 2–3 nm in height (8, 9). Like the mature amyloid fibrils, these intermediate aggregates have been suggested to cause cytotoxicity that leads to diseases (25–27). Although this type of protein aggregates has been termed “amorphous”, only small heterogeneity was observed in TEM and AFM (see Figure 4.2 and 4.3), arguing against complete disorder in the structure of these aggregates. Nevertheless, more experiments are required to probe if there is a specific pattern in structural organization of the LHCP aggregate.

How stable are the LHCP aggregates? This is an important question because it directly relates to the amount of energy cpSRP43 has to overcome during disaggregation, and hence provides a measure of the capacity of this chaperone as a disaggregase. Some protein aggregates, such as protein precipitates produced when the protein concentration exceeds the solubility limit (e.g., “salting out” effect) or the “soluble aggregates” formed

by oligomeric protein complexes, can be readily re-dissolved by dilution in fresh buffer and retain native conformations (28). This is not the case for highly stable amyloid fibrils, which are detergent-insoluble and could only be dissolved in strong chemical denaturants (29). The results here indicate that LHCP aggregates are stable both kinetically and thermodynamically. First, extensive dilution of the aggregate does not lead to re-solubilization (Figure 4.1A, red), suggesting that LHCP aggregates, once formed, are kinetically stable. Second, LHCP aggregates are resistant to a variety of detergents, even up to 2% SDS, and are solubilized only by strong chemical denaturants. Finally, both the protein concentration dependence of aggregate formation and the urea concentration dependence of re-solubilization of this aggregate are cooperative, suggesting cooperativity in the interactions that stabilize the aggregate. Importantly, quantitative analyses based on the urea solubilization curves provide an empirical method to assess the stability of the aggregates. This will allow us to systematically correlate perturbations in the stability of the aggregate with changes in the efficiency of the disaggregation reaction and can teach us about the roles that these internal packing interactions play in the disaggregation process mediated by cpSRP43.

Many questions remain to be addressed regarding the nature and structure of the LHCP aggregate. For instance, how many LHCP monomers reside in each aggregate particle? This question could be explored by STEM, in which the electron density from unstained samples is compared to that from the standard specimen with known oligomeric composition, and the mass-per-area can be calculated based on the electron density (10). This technique has been successful in calculating the number of A β peptides per length in the amyloid fibrils (8, 30). Another interesting question is whether

any secondary structures are present in the aggregate, and if so, what these structures are. The strong staining of ThT suggests the possibility that the aggregate could contain β -sheet rich areas since ThT prefers binding to cross- β strand structures (11). However, the native LHCP is a helical protein (19). This question can be explored further by Fourier-transformed infrared spectroscopy (FT-IR) or 2D-IR (31).

Yet the key question that is central to understanding the mechanism of cpSRP43's disaggregase activity is: what features of the LHCP aggregate allow cpSRP43 to recognize it and initiate the disaggregation process? Which parts of the LHCP are presented outside the aggregate, and which parts are buried inside? Although additional experimental evidence is required, the results here strongly suggest that the formation of LHCP aggregates involves hydrophobic collapse driven by the sequestering of its three TM helices. As a result, they might leave their more hydrophilic segments exposed to solvent, similar to the formation of detergent micelles. These parts would likely include the loops in between the TMs, especially the L18 motif. Indeed, preliminary results from chemical modification and electron paramagnetic resonance experiments have indicated that the L18 motif is solvent-exposed when LHCP forms aggregates (T.X. Nguyen, V. Q. Lam, unpublished data). As the L18 is the primary recognition element for cpSRP43, its exposure on the exterior of the aggregate provides a very attractive mechanism for how cpSRP43 could recognize and anchor onto the aggregate to start the disassembly process.

In summary, characterization of the LHCP aggregate is vital to understanding the molecular mechanism by which cpSRP43 reverses LHCP aggregation. For a disaggregase that is highly specific to its substrate, the nature of LHCP aggregates is key

to understanding the capacity and limitations of cpSRP43. Further experiments are necessary for elucidating higher-resolution architecture of this aggregate.

Materials and Methods

Materials. LHCP and LHCP mutants were purified under a denaturing condition as described (17). A β^{1-40} and re-crystallized ThT were generous gifts from Dr. J. W. Kelly. ANS and bis-ANS were purchased from Sigma and Invitrogen, respectively. LDAO, DDM, β -OG, and BNG were obtained from Anatrace. SDS was from BioRad. Urea and guanidinium chloride were molecular biology grade from MP and Sigma, respectively.

Light scattering. Light scattering experiments were performed as previously described (17). For formation of aggregates (Figure 4.1A, black), unfolded LHCP in 8M urea was directly diluted into Buffer D (50 mM K-HEPES pH 7.5, 200 mM NaCl) to the final concentration in each data point, controlling for equal final concentration of urea. For serial dilution experiments (Figure 4.1A, red), the sample at 1 μ M LHCP was serially diluted (by twofold) into fresh buffer D. The CMCs are obtained as the X-intercepts from linear fits of data from the aggregate formation concentration series.

TEM. LHCP aggregate was formed by diluting unfolded LHCP in 8M urea into Buffer D to the final concentration of 2 μ M. After incubation at 25 °C for 5 minutes, the sample was diluted fivefold and immediately deposited onto a glow-discharged 200-mesh Formvar grid (Ted Pella Inc., CA). After 45 second adsorption time, the grid was washed in water and then stained with 1% uranyl acetate for 45 seconds. TEM images were obtained on a 120 kV Tecnai T12 electron microscope coupled with a CCD camera. The diameters of the particles were measured using ImageJ (32).

AFM. 1 μ M LHCP aggregate in Buffer D was deposited onto a freshly-cleaved mica and incubated for 5 minutes at 25 °C to allow equilibration. The wafer was then rinsed with Millipore water and dried under the weak flux of nitrogen. AFM images were

immediately taken after the sample was prepared. A Digital Instrument Nanoscope IIIA AFM system in tapping mode was used throughout at ambient conditions. A sharp TESP tip (Veeco, CA) was used in the experiment. Typical values for the force constant, resonance frequency, and tip radius were 42 N/m, 320 kHz, and 8 nm, respectively. The distribution of particle sizes was obtained by calculating the projected area of each particle at half maximum height onto the surface. This is because the apparent *lateral* size of surface features is usually overestimated due to the broadening effect of the AFM tip. By taking the cross section area at half the maximum height, one can obtain a more realistic distribution of sizes of the particles.

Fluorescence. All fluorescence experiments were carried out in Buffer D using a Fluorolog 3-22 spectrofluorometer (Jobin Yvon). For bis-ANS experiments, 1 μM bis-ANS was added to Buffer D with or without 1 μM LHCP aggregate. The samples were excited at 395 nm and then scanned from 410 to 620 nm, with the excitation and emission band passes of 2 and 5 nm, respectively. For ThT experiments, 20 μM re-crystallized ThT was added to Buffer D containing no aggregate, aggregates from 1 or 5 μM LHCP, or 15 μM freshly-sonicated $\text{A}\beta^{1-40}$. The samples were excited at 440 nm and then scanned from 470 to 570 nm, with the excitation and emission band passes of 3 and 7 nm, respectively. For comparison, ThT fluorescence from 1 and 5 μM unfolded LHCP in 8M urea were measured.

Sedimentation assay. Unfolded LHCP was diluted to 10 μM in Buffer D and incubated at 25 °C for 5 minutes. Aggregation was complete, judged by the absence of LHCP in the supernatant after centrifugation at 13,000 rpm in a microfuge for 30 minutes. The pellet was dissolved with 50 μl of various detergent or chemical denaturants at different

concentrations for 30 minutes at 25 °C. The mixtures were then spun at 13,000 rpm in a microfuge for 30 minutes, and soluble (S) and pellet (P) fractions were visualized by SDS-PAGE.

For Figure 4.6B, the intensity of the Coomassie-stained bands were quantified using ImageJ (32). The data were fit with a function derived from the two-state model for protein folding (33), shown below:

$$\theta = \frac{1}{1 + e^{-m(U_{50} + [\text{urea}])/RT}} \quad (1)$$

where θ is the fraction soluble [$s/(s+p)$], R is the gas constant, and T is temperature. The fit gave U_{50} , which is the urea concentration at which 50% of LHCP aggregate was solubilized, and m , which represents a constant of proportionality. ΔG° , which represents free energy of transfer of the aggregate from water to urea, could be calculated from fits to eq 5 ($= -mU_{50}$).

SDS solubility assay. For Figure 4.5B, the assay was performed as described for amyloid fibrils (24). Briefly, aggregation of 10 μ M LHCP in Buffer D proceeded for 5 minutes at 25 °C. The mixture was then mixed with 2% SDS-PAGE loading buffer and either incubated at 25 °C or boiled at 100 °C for ten minutes prior to gel loading. Total mixture was loaded without centrifugal separation, and only the proteins that migrated into the separating gel (e.g., solubilized portion) were visualized.

Acknowledgement.

We thank A.N. Murray and Dr. J.W. Kelly for re-crystallized ThT and A β^{1-40} , and Dr. A. McDowell and P. Cao for extensive help with TEM and AFM analyses, respectively.

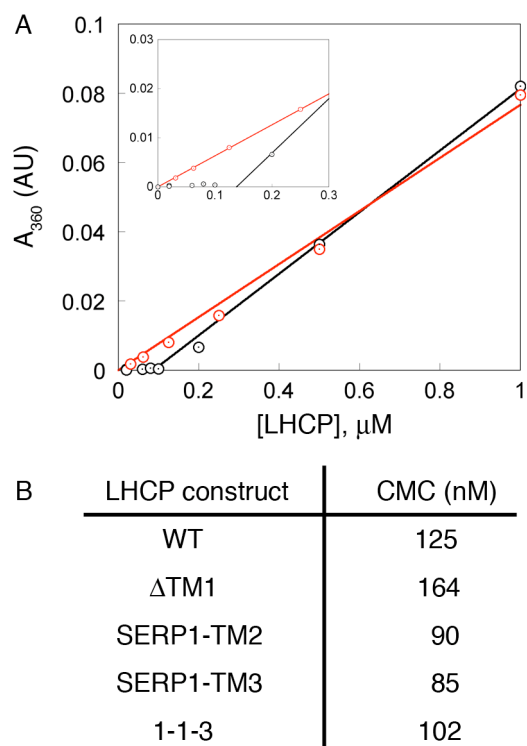


Figure 4.1 LHCP forms aggregates after a critical concentration. (A) Formation of the LHCP involves a lag phase. Light scattering intensities during formation of the aggregate (black) are compared to those obtained from serial dilution of pre-formed aggregates (red). The inset highlights the lag phase at low concentrations that is only present during formation of the aggregate. (B) Summary of the CMC values of aggregate formation by different LHCP mutants.

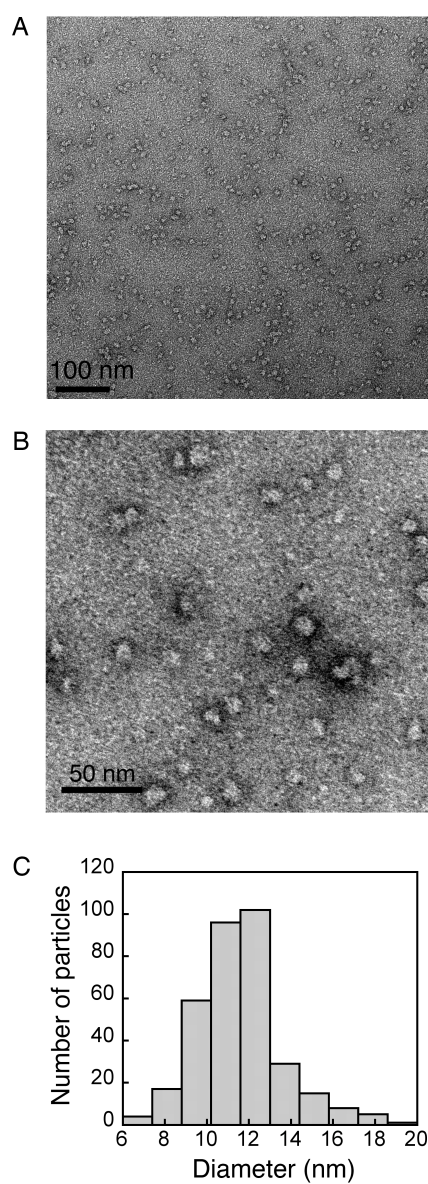


Figure 4.2 TEM analysis of LHCP aggregates. (A) Large-field view of a negatively stained TEM image of LHCP aggregates shows well-separated and similarly sized particles. (B) A zoomed-in image shows that LHCP aggregates are round-shaped particles. (C) Distribution of the diameter of LHCP aggregates, measured from several independent experiments. The mean diameter is 12 ± 2 nm.

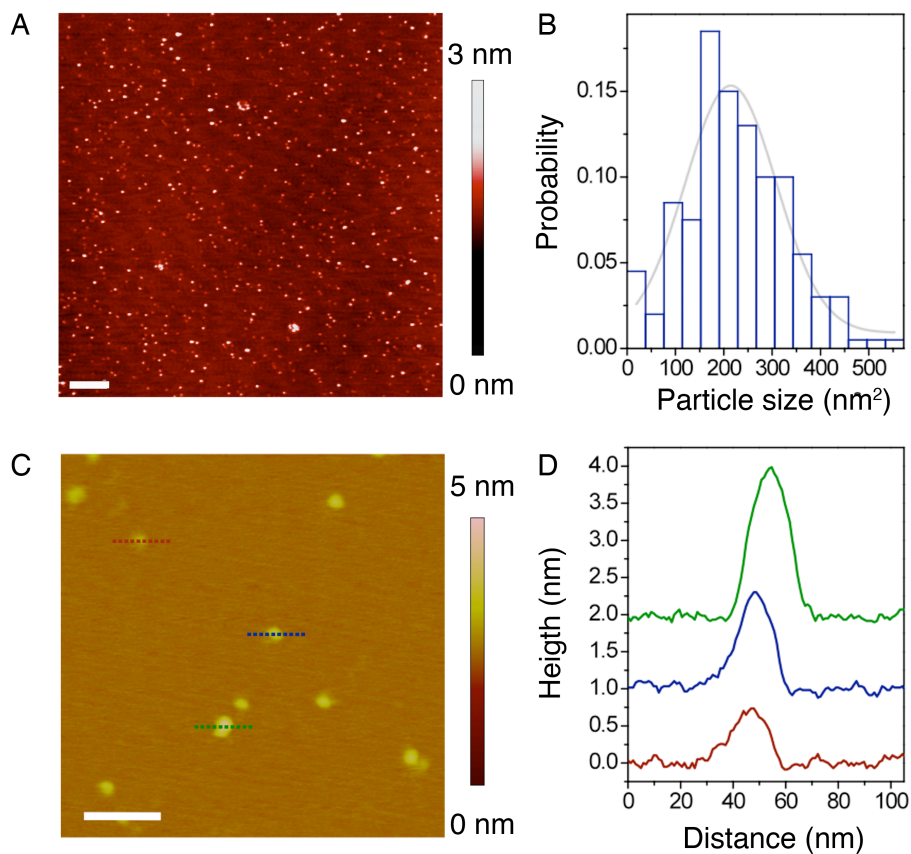


Figure 4.3 AFM analysis of LHCP aggregates. (A) Large-field view of AFM topographic image shows well-separated LHCP aggregates. Large clusters are occasionally observed. The scale bar is 500 nm. (B) Distribution of the area of LHCP aggregates, measured from several regions on the surface. The gray line is a Gaussian fit to the data, which gave a mean area of the particle of 214 nm². (C) A zoomed-in region of the image reveals disc-shaped particles. The lines indicate particles whose heights were measured (red, blue, and green). The scale bar is 100 nm. (D) The height profiles for the particles indicated in C. Curves are vertically displaced for clarity.

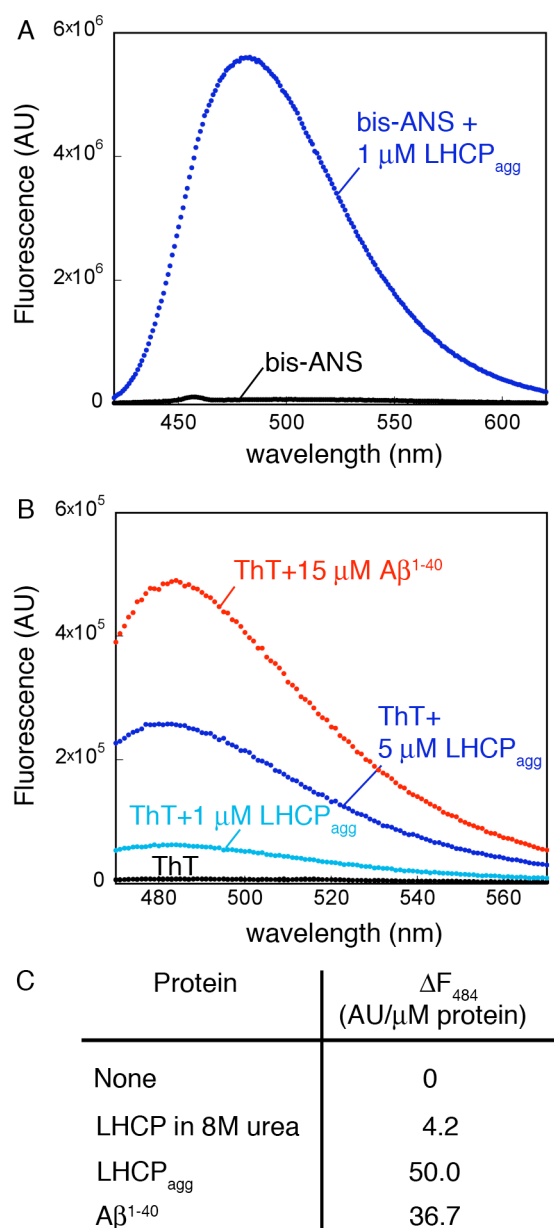


Figure 4.4 LHCP aggregates contain exposed hydrophobic surfaces as probed by small molecule dyes. (A) Fluorescence emission spectra of 1 μM bis-ANS with (blue) or without (black) 1 μM LHCP aggregate. (B) Fluorescence spectra of 20 μM ThT in the absence (black) and presence of 1 (light blue) or 5 (dark blue) μM LHCP aggregate, or 15 μM A β^{1-40} (red). (C) ThT fluorescence change at 484 nm per μM of protein.

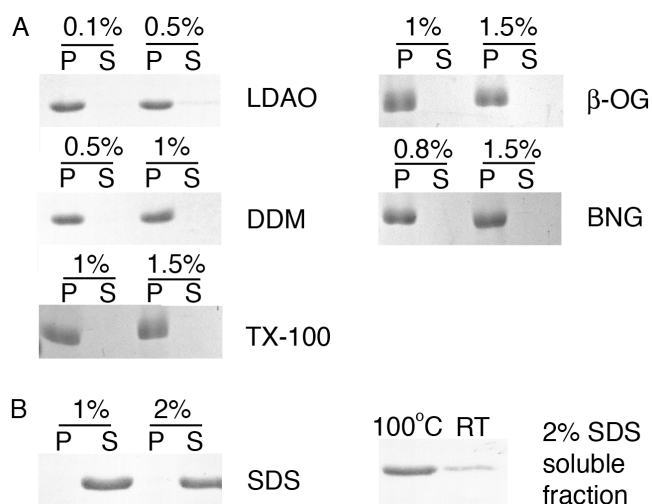


Figure 4.5 LHCP aggregates are resistant to many detergents. (A) Sedimentation analysis of the ability of various detergents to resolubilize LHCP aggregates. P and S denote the pellet and soluble fractions, respectively. (B) Sedimentation analysis (left) and SDS-solubility assay as described for amyloids ((24); right) show partial solubility of LHCP aggregates in 2% SDS. In the left panel, the samples were centrifuged to separate pellet and soluble fractions and boiled prior to gel loading. In the right panel, the samples were not separated by centrifugation, and solubility was judged by the mobility of the protein band into the separating gel. Quantification using ImageJ revealed that 24% of the LHCP aggregate is soluble when the sample was not boiled (RT), compared to 87% for the boiled sample (100 °C).

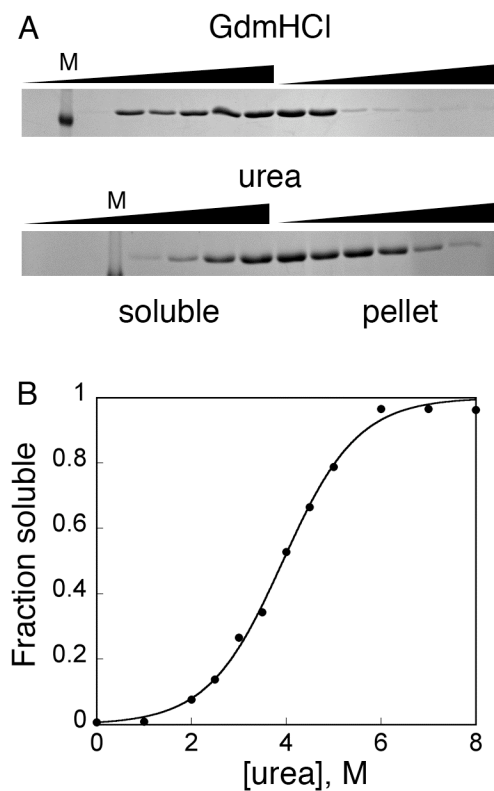


Figure 4.6 LHCP aggregates can be re-solubilized by chemical denaturants. (A) Sedimentation analysis of the ability of guanidinium chloride (GdmHCl) and urea to re-solubilize LHCP aggregates. ‘M’ denotes the protein marker lane. (B) Quantification of the solubilized fraction revealed a cooperative dependence on urea concentration. The fit to eq 1 gave a ΔG^0 of 2.9 kcal/mol and a U_{50} of 3.93 M.

References:

1. Hayer-Hartl, M., and Hartl, F.U. (2002) Molecular chaperones in the cytosol: from nascent chain to folded protein, *Science* 295, 1852–1858.
2. Luheshi, L. M., and Dobson, C.M. (2009) Bridging the gap: from protein misfolding to protein misfolding diseases, *FEBS Lett.* 583, 2581–2586.
3. Zettlmeissl, G., Rudolph, R., and Jaenicke, R. (1979) Reconstitution of lactic dehydrogenase. Noncovalent aggregation vs. reactivation. 1. Physical properties and kinetics of aggregation, *Biochemistry* 18, 5567–5571.
4. Kopito, R. R. (2000) Aggresomes, inclusion bodies and protein aggregation, *Trends in Cell Biology* 10, 524–530.
5. Brems, D. N., Plaisted, S.M., Havel, H.A., and Tomich, C.S.C. (1988) Stabilization of an associated folding intermediate of bovine growth hormone by site-directed mutagenesis, *Proc. Natl. Acad. Sci. USA* 85, 3367–3371.
6. Speed, M. A., Wang, D.I.C., and King, J. (1996) Specific aggregation of partially folded polypeptide chains: The molecular basis of inclusion body composition, *Nature Biotechnology* 14, 1283–1287.
7. Nelson, R., Sawaya, M.R., Balbirnie, M., Madsen, A.Ø., Riek, C., Grothe, R., and Eisenberg, D. (2005) Structure of the cross-beta spine of amyloid-like fibrils, *Nature* 435, 773–778.
8. Goldsbury, C., Wirtz, S., Muller, S.A., Sunderji, S., Wicki, P., Aepli, U., and Frey, P. (2000) Studies on the *in vitro* assembly of A β 1–40: Implications for the search for A β fibril formation inhibitors, *J. Struct. Biol.* 130, 217–231.
9. Mastrangelo, I., Ahmed, M., Sato, T., Liu, W., Wang, C., Hough, P., and Smith, S.O. (2006) High-resolution atomic force microscopy of soluble A β 42 oligomers, *J. Mol. Biol.* 358, 106–119.
10. Wall, J. S., and Hainfeld, J.F. (1986) Mass mapping with the scanning transmission electron microscope, *Annu. Rev. Biophys. Biophys. Chem.* 15, 355–376.
11. LeVine, H. I. (1999) Quantification of beta-sheet amyloid fibril structures with thioflavin T., *Methods Enzymol.* 309, 274–284.
12. Stryer, L. (1965) The interaction of a naphthalene dye with apomyoglobin and apohemoglobin. A fluorescent probe of non-polar binding sites, *J. Mol. Biol.* 13, 482–495.
13. Ivanova, M. I., Sievers, S.A., Sawaya, M.R., Wall, J.S., and Eisenberg, D. (2009) Molecular basis for insulin fibril assembly, *Proc. Natl. Acad. Sci. USA* 106, 18990–18995.
14. Doyle, S. M., and Wickner, S. (2008) Hsp104 and ClpB: protein disaggregating machines, *Trends Biochem. Sci.* 34, 40–48.
15. Glover, J. R., and Lindquist, S. (1998) Hsp104, Hsp70, and Hsp40: a novel chaperone system that rescues previously aggregated proteins, *Cell* 94, 73–82.
16. Doyle, S. M., Hoskins, J.R., and Wickner, S. (2007) Collaboration between the ClpB AAA+ remodeling protein and the DnaK chaperone system, *Proc. Natl. Acad. Sci. USA* 104, 11138–11144.

17. Jaru-Ampornpan, P., Shen, K., Lam, V.Q., Ali, M., Doniach, S., Jia, T.Z., and Shan, S. (2010) ATP-independent reversal of a membrane protein aggregate by a chloroplast SRP subunit, *Nat. Struct. Mol. Biol.* 17, 696–702.
18. Schuenemann, D., Gupta, S., Persello-Cartieaux, F., Klimyuk, V. I., Jones, J. D. G., Nussaume, L., and Hoffman, N. E. (1998) A novel signal recognition particle targets light-harvesting proteins to the thylakoid membranes, *Proc. Natl. Acad. Sci. USA* 95, 10312–10316.
19. Liu, Z., Yan, H., Wang, K., Kuang, T., Zhang, J., Gui, L., An, X., and Chang, W. (2004) Crystal structure of spinach major light-harvesting complex at 2.72 Å resolution, *Nature* 428, 287–292.
20. Delille, J., Peterson, E. C., Johnson, T., Morre, M., Kight, A., and Henry, R. (2000) A novel precursor recognition element facilitates posttranslational binding to the signal recognition particle in chloroplasts, *Proc. Natl. Acad. Sci.* 97, 1926–1931.
21. Tu, C. J., Peterson, E. C., Henry, R., and Hoffman, N. E. (2000) The L18 domain of light-harvesting chlorophyll proteins binds to chloroplast signal recognition particle 43, *J. Biol. Chem.* 275, 13187–13190.
22. Hurshman, A. R., White, J.T., Powers, E.T., and Kelly, J.W. (2004) Transthyretin aggregation under partially denaturing conditions is a downhill polymerization, *Biochemistry* 43, 7365–7381.
23. Groenning, M., Olsen, L., van de Weert, M., Flink, J.M., Frokjaer, S., and Jorgensen, F.S. (2007) Study on the binding of Thioflavin T to β -sheet-rich and non- β -sheet cavities, *J. Struct. Biol.* 158, 358–369.
24. Chernoff, Y. O., Uptain, S.M., and Lindquist, S.L. (2002) Analysis of prion factors in yeast, *Methods Enzymol.* 351, 499–538.
25. McLean, C. A., Cherny, R.A., Fraser, F.W., Fuller, S.J., Smith, M.J., Beyreuther, K., Bush, A.I., and Masters, C.L. (1999) Soluble pool of A β amyloid as a determinant of severity of neurodegeneration in Alzheimer's disease, *Ann. Neurol.* 46, 860–866.
26. Walsh, D. M., Klyubin, I., Fadeeva, J.V., Cullen, W.K., Anwyl, R., Wolfe, M.S., Rowan, M.J., and Selkoe, D.J. (2002) Naturally secreted oligomers of amyloid- β protein potently inhibit hippocampal long-term potentiation *in vivo*, *Nature* 416, 535–539.
27. Dahlgren, K. N., Manelli, A.M., Stine, W.B. Jr, Baker, L.K., Krafft, G.A., and LaDu, M.J. (2002) Oligomeric and fibrillar species of amyloid- β peptides differentially affect neuronal viability, *J. Biol. Chem.* 277, 32046–32053.
28. Fink, A. L. (1998) Protein aggregation: folding aggregates, inclusion bodies and amyloid, *Folding and Design* 3, 9–23.
29. Serio, T. R., Cashikar, A.G., Kowal, A.S., Sawicki, G.J., Moslehi, J.J., Serpell, L., Arnsdorf, M.F., and Lindquist, S.L. (2000) Nucleated conformational conversion and the replication of conformational information by a prion determinant, *Science* 289, 1317–1321.
30. Sen, A., Baxa, U., Simon, M.N., Wall, J.S., Sabate, R., Saupe, S.J., and Steven, A.C. (2007) Mass analysis by scanning transmission electron microscopy and

electron diffraction validate predictions of stacked β -solenoid model of HET-s prion fibrils, *J. Biol. Chem.* 282, 5545–5550.

31. Strasfeld, D. B., Ling, Y.L., Gupta, R., Raleigh, D.P., and Zanni, M.T. (2009) Strategies for Extracting Structural Information from 2D IR Spectroscopy of Amyloid: Application to Islet Amyloid Polypeptide, *J. Phys. Chem. B* 113, 15679–15691.
32. Abramoff, M. D., Magelhaes, P.J., and Ram, S.J. (2004) Image Processing with ImageJ, *Biophotonics International* 11, 36–42.
33. Fersht, A. (1998) *Structure and mechanism in protein science: a guide to enzyme catalysis and protein folding*, W.H. Freeman and Company, New York.